Evaluation of the Effect of a Tracheal Stent on Radiation Dose Distribution via Micro-CT Imaging

Tao Lin, MS[1,2,3], Xinye Ni, PhD[2,3], Liugang Gao, MS[2,3], Jianfeng Sui, MS[2,3], Kai Xie, MS[2,3], and Shuquan Chang, PhD[1]

Abstract

Purpose: To study the effect of a metal tracheal stent on radiation dose distribution. **Method:** A metal tube bracket is placed in a self-made foam tube sleeve, and micro-computed tomography scanning is performed directly. The foam sleeve containing the metal bracket is placed in a nonuniform phantom for a routine computed tomography scan. The stents in conventional computed tomography images are replaced by the stents in micro-computed tomography images. Subsequently, 2 sets of computed tomography images are obtained and then imported to a radiotherapy treatment planning system. A single photon beam at $0°$ is designed in a field size of 10 cm × 10 cm, a photon beam of 6 MV, and a monitor unit of 200 MU. Monte Carlo algorithm is used to calculate the dose distribution and obtain the dose curve of the central axis of the field. The dose is verified with thermo-luminescence dose tablets. **Results:** The micro-computed tomography images of the tracheal stent are clearer and less false-like than its conventional computed tomography images. The planned dose curves of the 2 groups are similar. In comparison with the images without any stents in place, the doses at the incident surface of the stent in the conventional computed tomography images and at the stent exit surface in the rear of the stent increase by 1.86% and 2.76%, respectively. In the micro-computed tomography images, the doses at the incident surface of the stent and at the exit surface behind the stent increase by 1.32% and 1.19%, respectively. Conventional computed tomography reveals a large deviation between the measured and calculated values. **Conclusion:** Tracheal stent based on micro-computed tomography imaging has a less effect on radiotherapy calculation than that based on conventional computed tomography imaging.

Keywords
CT images, dose, micro-CT, tracheal stent, radiation

Abbreviations
CC, collapsed cone; CT, computed tomography; FOV, field of view; TPS, treatment planning system; PB, pencil beam

Received: October 25, 2018; Revised: February 02, 2019; Accepted: March 26, 2019.

Introduction

Tracheal bronchial stent can expand and improve a narrow airway. When patients with lung cancer and complications, such as airway obstruction, chronic asphyxia, and obstructive pneumonia, are treated with tracheobronchial stents, the symptoms of dyspnea can be immediately relieved, and ventilation function and quality of life can be significantly improved.[1,2] Accordingly, further treatment can be formulated and clinically applied.

When patients with a tracheal or bronchial stent undergo radiotherapy, metal artifacts generated by the metal component

[1] College of Materials Science and Technology, Nanjing University of Aeronautics and Astronautics, Nanjing, China
[2] Department of Radiation Oncology, Changzhou No. 2 People's Hospital, Nanjing Medical University, Changzhou, China
[3] The Center for Medical Physics of Nanjing Medical University, Changzhou, China

Corresponding Author:
Xinye Ni, PhD, Department of Radiation Oncology, Changzhou No. 2 People's Hospital, Nanjing Medical University, Xinglong Street 29#, Changzhou 213003, China.
Email: nxy@njmu.edu.cn

of the stent and conventional computed tomography (CT) scan cause a dose disturbance at the junction of the stent and surrounding tissues. Moreover, changes in doses at the junction can affect the tumor control rate. The effect of metal stents on dose has been studied in detail. For instance, the effect of metal stent on dose mainly depends on metallic materials, density of grids, and size of metal artifacts.[3,4]

Abu Dayyeh[4] analyzed the effect of different materials on the radiation dose for esophageal cancer. The effect of nonmetallic and stainless steel stents on doses is greater than that of nickel–titanium alloy metal stents. The effect of the grid density of stents on dose is more remarkable than that of metallic materials, and the effect of a high-density grid on dose disturbance is greater than that of a low-density grid. The effect of dose deviation on the adverse reactions of the trachea needs further clinical observation and can be reduced by designing multiple radiation fields in different directions.[5,6] Evans studied the effect of a metal tracheal stent on dose and conducted an animal experiment involving the implantation of the stent to the trachea of pigs for irradiation. The measured radiation dose of the metal tracheal stent on the trachea and surrounding tissues varies from 1.8% to 6.1% within the range of 5% measurement error and without a significant difference.[7]

Most studies are based on conventional CT, but conventional CT is unsuitable for microscopic stent imaging because it produces images with insufficient resolution and generates artifacts. Conversely, micro-CT has a high resolution of 1 to 100 μm, has a good microscopic function, and can obtain clear scanning images. Micro-CT adopts a tapered beam X-ray, which can obtain isotropic volumetric images and improve spatial resolution and X-ray utilization. It is widely used in tumor measurement, blood vessel extraction, and material analysis.[8,9] In our study, micro-CT is used to scan a metal scaffold and analyze the effect of tracheal stent on dose during radiotherapy. The difference between the calculated value of the planning system and the actual measured value is compared through thermoluminescence dosimetry.

Materials and Methods

1. Experimental materials: The tracheal stent is made of Nitinol (Nanjing Minimally Invasive Medical Technology Co, Ltd, China), which is woven in a mesh similar to a Nitinol memory alloy wire with a diameter of 0.2 to 0.3 mm. The following instruments are used: SOMATOM Definition Flash CT machine (Siemens, Munich, Germany), Skyscan1176 Micro-CT tomography system (Bruker, Kontich, Belgium), THORAX002LFC nonuniform mold (American CIRS Company, Virginia), TLD FJ-427A$_1$ microcomputer thermoluminescence-measuring instrument (Beijing Nuclear Instrument Factory, China), Infinity linear accelerator, and Monaco planning system (V5.3; Elekta, Stockholm, Sweden).

2. Material processing and CT scanning: A foam is processed into a hollow cylinder with an internal diameter

Figure 1. Mold with a tracheal stent.

Figure 2. Location of TLDs.

of 1.5 cm and an external diameter of 2.5 cm based on the dimensions of the inserted holes and the tracheal stents in the nonuniform mold of CIRS. The stent is placed into it and then into the micro-CT for scanning. The source voltage is 80 kV. Then, the stent is placed into the mold body (Figure 1) for CT scanning under a scanning condition of 80 kV/120 mAs. The width of the scanning collimator is 0.6 mm × 64 mm, and the scanning mode is set at spiral scanning with a thickness of 1 mm. After scanning is completed, the CT images are sent to the Monaco planning system through the network. Matlab 8.3 is used to process images and replace the stent image obtained through micro-CT scanning by the one obtained through conventional CT scanning. The CT value of the micro-CT image is corrected on the basis of the CT value of the stent in the positioning CT image. The processed image is subsequently imported into the Monaco planning system.

3. Program planning: A single front view of 0° is designed for 2 kinds of images. The energy is 6 MV, the beam field size is 10 cm × 10 cm, with source–axis distance (SAD) = 100 cm. The center axis of the field passes through the center of the holder, the monitor unit is 200 MU, and the Monte Carlo algorithm is used. The calculated grid spacing is 0.1 cm, and the statistical uncertainty is 0.1%.

4. Measurement: A TLD is pasted around the surface of the tracheal stent (Figure 2A-D) and then placed into the mold. TLD chips are prescreened by repeated
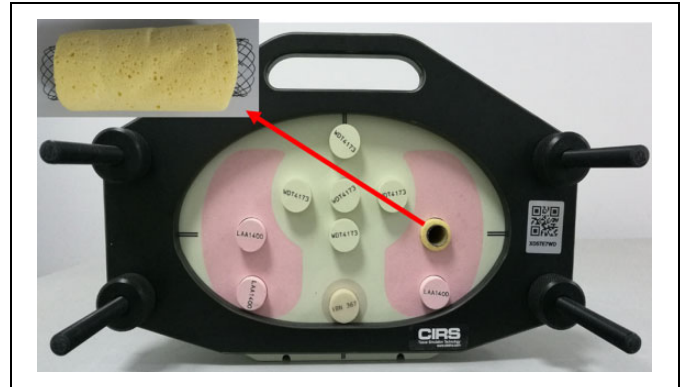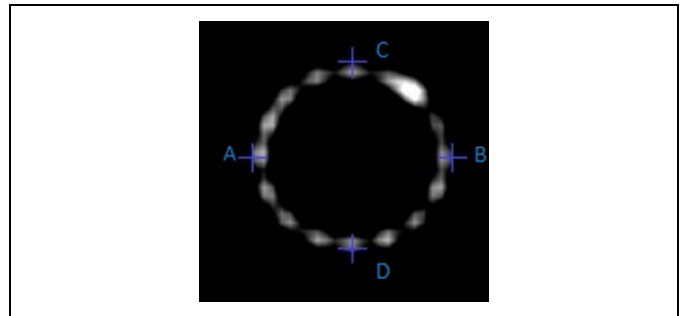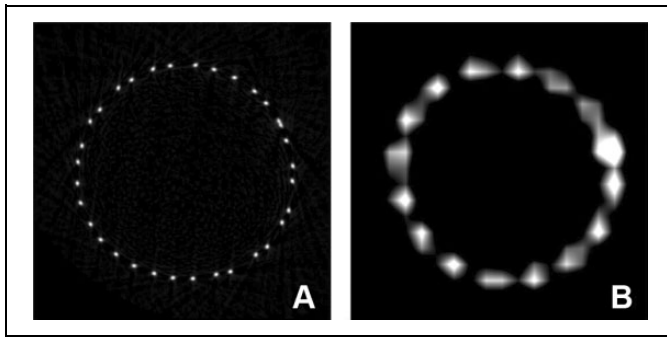
Figure 3. Micro-CT (A) and conventional CT (B) images of a metallic tracheal stent. CT indicates computed tomography.

radiation at 200 to 500 cGy, and only the chips showing small measurement uncertainties (within 4%) are selected to ensure the accuracy of the measurements.[10] The mold containing the TLD is placed as planned and irradiated under a linear accelerator. The measurement is repeated 5 times, and data are read by a thermoluminescence instrument. The average value is taken.

5. Dose drawing processing and analysis: The 2 groups of plans are imported into Matlab 8.3 (US MathWorks Company, Massachusetts) via the flux chart of the horizontal surface of the central axis of the field. Then, a vertical line is taken through the metal bracket for each image, and the dose value is obtained on the vertical line.

Results

The metal stents scanned by conventional CT and micro-CT are shown in Figure 3. In conventional CT images, the stent structure is visible and the artifacts are heavy. In micro-CT images, the scaffold structure is clear and the artifacts are small.

Figure 4 shows the dose distribution of the 2 groups. In particular, the dose curve of the 2 groups is similar, and the distribution of the dose curve around the stent varies. The dose curve of the conventional CT image group is tightened around the stent.

Figure 5 shows the depth–dose curve of the center axis of the overshooting field at the central plane of the 2 groups. Dose peaks are detected at the incident face of the stent. The peak width of the dose peak around the stent in the depth–dose line planned in the conventional CT group is wider than that in the micro-CT group. The following equation is used to quantitatively compare the effects of the stent on dose and to calculate the effects of stent implantation on dose: $A = \frac{PDD_{stent} - PDD_{no\ stent}}{PDD_{no\ stent}}$, where PDD_{stent} and $PDD_{no\ stent}$ represent the 100% depth dose of the mold body with and without the stent, respectively. The dose in conventional CT images increases by 1.86% at the incident surface because of the stent placement and by 2.76% at the second incident surface behind the stent compared with that of the untreated stent module. In micro-CT images, the dose increases by 1.32% at the incident surface because of the stent placement and by 1.19% at the second incident surface behind the stent.

Table 1 shows the TLD data after the actual irradiation and the calculated value of the treatment planning system (TPS) at the location. The difference between the measured and calculated values is equal to (measured value − calculated value)/ measured value, and the difference between the 2 is less than 5%. Within the measurement error range of thermoluminescence dosing tablets, the difference between the calculated and measured values of the micro-CT image group is smaller than that of the conventional CT image group.

Discussion

The therapeutic planning system calculates the dose deposition of radiation in a patient's body on the basis of the relative
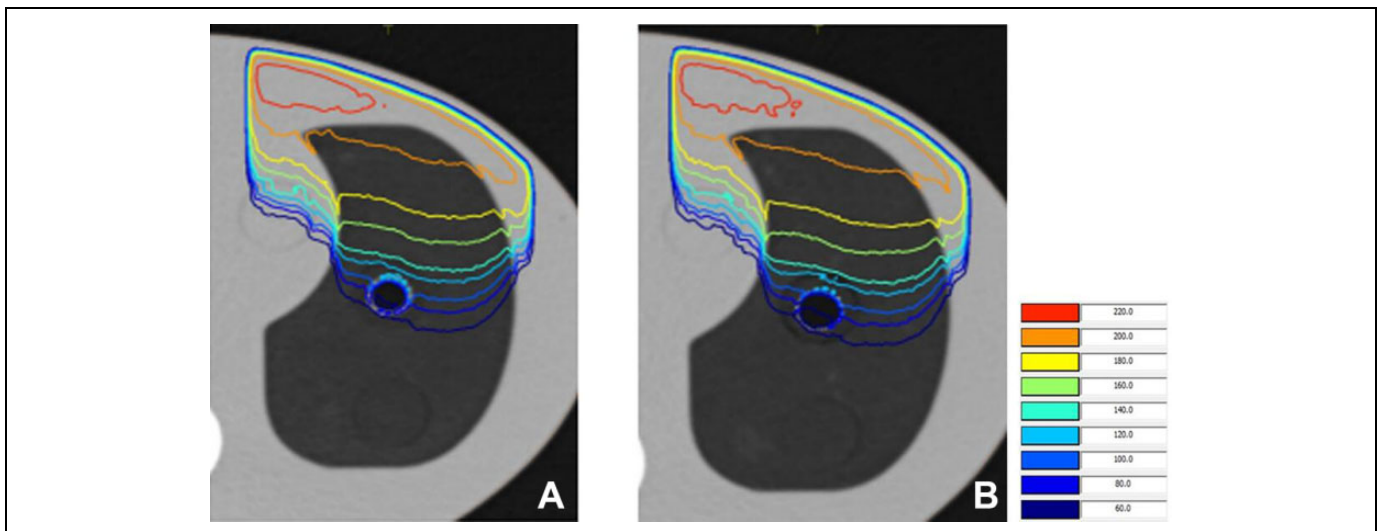

Figure 4. Conventional CT images (A) and micro-CT images (B) of dose distribution. CT indicates computed tomography.
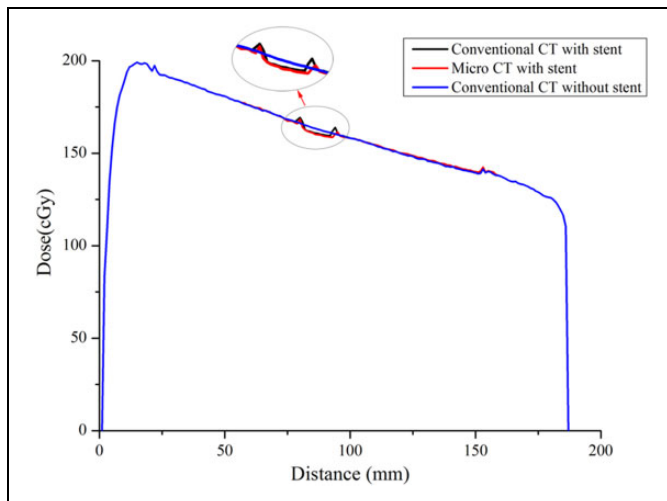
Figure 5. Depth–dose curve of the central axis of the overshooting field at the central level of the conventional CT and micro-CT image planning. CT indicates computed tomography.

Table 1. Differences Between the Measured Values of Thermoluminescence Dosage Tablets and the Calculated Values of TPS.

Dose Point	Measured Value (cGy)	Conventional CT		Micro-CT	
		Calculated Value (cGy)	Differences	Calculated Value (cGy)	Differences
A	164.2 ± 3.8	158.9	3.2%	161.9	1.4%
B	167.6 ± 3.5	161.4	3.7%	164.4	1.9%
C	171.8 ± 2.8	163.7	4.7%	167.2	2.7%
D	163.8 ± 3.1	157.3	4.0%	161.1	1.6%

Abbreviations: CT, computed tomography; TPS, treatment planning system.

electron density of each body part. The relative electron density is derived from a CT image, which is transformed by the CT value–electron density curve.[11,12] The correct reading of a CT value is directly related to the accuracy of dose calculation. Metal artifacts are generated during conventional CT scanning of metal stents, and metallic stents appear thick in CT images, thereby affecting the CT value of a stent and its surrounding tissues. Micro-CT scanning can obtain isotropic volumetric images with high spatial resolution by using a cone X-ray beam. In this study, micro-CT is used to scan the metal stent, and the stent images are reduced compared with those of conventional CT scanning.

When the conventional CT scan phantom was performed, the voxel contains metal scaffolds and substitutes lung tissue, which has 2 kinds of density differences that produce a partial volume effect, because of the thickness of the scan layer. The scanning layer in a micro-CT scan is thinner than that in the conventional CT. The partial volume effect and the display rate of the stent are also greatly improved in the micro-CT scan.

The quality of CT images is related to their resolution, which is divided into spatial resolution and resolution. Spatial resolution is associated with equipment, scanning layer thickness, field of view (FOV), and image reconstruction algorithms. The thinner the scanning layer is, the smaller the voxel, the more difficult the production of partial volume effect, and the stronger the ability of an image to show small structures will be. The size of the FOV determines the image pixel size, that is, the smaller the FOV is, the more the pixels and the sharper the image will be. Conventional CT generally adopts fan-shaped X-ray beams, whereas micro-CT usually applies cone X-ray beams. A cone beam can obtain the true isotropic volume image and improve the spatial resolution. Micro-CT adopts a micro focus that is different from that of conventional CT, and its resolution can reach a micron level. It also has a good "microscopic" effect. The FOV of micro-CT is much smaller than that of conventional CT, and the resulting image quality is stronger than that of conventional CT.

When radiation enters the mold from a high-density area to a low-density area, a dose drop effect is produced because the secondary electron flux changes as the ray enters the low-density region from the high-density region. A dose peak is generated behind it because of the gap between the 2 materials in the mold. The density of materials simulating the lung tissue is higher than that of air. Radiation enters the relatively high-density-simulated lung tissue from the low-density gap, forming a secondary build effect within the range of secondary electrons. The dose increases gradually as the depth increases. Conversely, the dose decreases after the effect is weakened beyond the maximum range. When incident photons pass through metal stents, an electron imbalance occurs at the incident surface. Scattering lines and secondary electrons in metal stents penetrate tissues by the backscattering of metal materials, thereby increasing the dose at the incident surface. Li[13] used an Monto Carlo (MC) model and demonstrated that the presence of esophageal metal scaffolds during esophageal cancer radiotherapy causes a 14% to 21% increase in the dose at 0.5 cm of the esophageal wall. The backscattering of metal implants is related to the material property of implants, such as the size of atomic number measured by a metal. The larger the atomic number is, the larger the scattering in the cross-section will be.[14] Abu Dayyeh[4] studied the effects of 6, 10, and 18 MV on backscattering and found no significant difference among the effects of the 3 levels on the backscattering of metal stents. Different algorithms have yielded various results on the surface dose of metal stents. The commonly used algorithms for planning systems include pencil beam (PB), collapsed cone (CC), and MC algorithm. For the dose calculation of metal implants, the CC algorithm is more accurate than the PB algorithm.[15] In this study, the MC algorithm is the most accurate for calculating the radiation dose distribution of metal implants.[16-18]

The dose increases at the exit surface of the stent because of the scattering lines and secondary electrons generated by the original rays passing through the metal stent. The dose increases gradually as the depth increases. By contrast, the dose decreases after the effect is weakened beyond the maximum range. A peak curve is shown in the depth–dose curve at the exit surface of the stent.

In this study, the actual measured value slightly differs from the results of TPS by the MC algorithm. Within the measurement error range, this algorithm can accurately calculate the radiation dose on the surface of metal implants. The surface dose of the metal scaffold increases by 1.32%, and the dose disturbance can be further reduced through the design of multiple directional radiation fields.

Conclusion

Tracheal stent images obtained by micro-CT are clearer than those produced by conventional CT scan. The influence of tracheal stent based on a micro-CT image on the calculated result of radiotherapy is less than that based on a conventional CT image.

Authors' Note

The presented data is summarized in this paper. The complete data sets can be retrieved from the authors upon formal request from interested readers. This study has not been done on humans or animals.

Declaration of Conflicting Interests

The author(s) declared no potential conflicts of interest with respect to the research, authorship, and/or publication of this article.

Funding

References

1. Tojo T, Iioka S, Kitamura S, et al. Management of malignant tracheobronchial stenosis with metal stents and Dumon stents. *Ann Thorac Surg*. 1996;61(4):1074-1078.

2. Tan BS, Watkinson AF, Dussek JE, Adam AN. Metallic endo-prostheses for malignant tracheobronchial obstruction: initial experience. *Cardiovasc Intervent Radiol*. 1996;19(2):91-96.

3. Liugang G, Hongfei S, Xinye N, Mingming F, Zheng C, Tao L. Metal artifact reduction through MV CBCT and kVCT in radiotherapy. *Scientific Reports*. 2016;6:37608.

4. Abu Dayyeh BK, Vandamme JJ, Miller RC, Baron TH. Esophageal self-expandable stent material and mesh grid density are the major determining factors of external beam radiation dose perturbation: results from a phantom model. *Endoscopy*. 2013;45(1): 42-47.

5. Gez E, Cederbaum M, Yachia D, Bar-Deroma R, Kuten A. Dose perturbation due to the presence of a prostatic urethral stent in patients receiving pelvic radiotherapy: an in vitro study. *Med Dosim*. 1997;22(2):117-120.

6. Chen YK, Schefter TE, Newman F. Esophageal cancer patients undergoing external beam radiation after placement of self-expandable metal stents: is there a risk of radiation dose enhancement? *Gastrointest Endosc*. 2011;73(6):1109-1114.

7. Evans AJ, Lee DY, Jain AK, et al. The effect of metallic tracheal stents on radiation dose in the airway and surrounding tissues. *J Surg Res*. 2014;189(1):1-6.

8. De Clerck NM, Meurrens K, Weiler H, et al. High-resolution X-ray microtomography for the detection of lung tumors in living mice. *Neoplasia*. 2004;6(4):374-379.

9. Wan SY, Kiraly AP, Ritman EL, Higgins WE. Extraction of the hepatic vasculature in rats using 3-D micro-CT images. *IEEE Trans Med Imaging*. 2000;19(9):964-971.

10. Xin-ye N, Xiao-bin T, Chang-ran G, Da C. The prospect of carbon fiber implants in radiotherapy. *J Appl Clin Med Phys*. 2012;13(4): 152-159.

11. Constantinou C, Harrington JC, DeWerd LA. An electron density calibration phantom for CT-based treatment planning computers. *Medical Physics*. 1992;19(2):325-327.

12. Saw CB, Loper A, Komanduri K, Combine T, Huq S, Scicutella C. Determination of CT-to-density conversion relationship for image-based treatment planning systems. *Med Dosim*. 2005; 30(3):145-148.

13. Li XA, Chibani O, Greenwald B, Suntharalingam M. Radiotherapy dose perturbation of metallic esophageal stents. *Int J Radiat Oncol Biol Phys*. 2002;54(4):1276-1285.

14. Ravikumar M, Ravichandran R, Sathiyan S, Supe SS. Backscattered dose perturbation effects at metallic interfaces irradiated by high-energy X- and gamma-ray therapeutic beams. *Strahlenther Onkol*. 2004;180(3):173-178.

15. Wieslander E, Knöös T. Dose perturbation in the presence of metallic implants: treatment planning system versus Monte Carlo simulations. *Phys Med Biol*. 2003;48(20):3295-3305.

16. Chetty IJ, Curran B, Cygler JE, et al. Report of the AAPM task group no. 105: issues associated with clinical implementation of Monte Carlo-based photon and electron external beam treatment planning. *Medical Physics*. 2007;34(12):4818-4853.

17. Verhaegen F, Seuntjens J. Monte Carlo modelling of external radiotherapy photon beams. *Phys Med Biol*. 2003;48(48): R107-R164.

18. Reynaert N, Marck SCVD, Schaart DR, et al. Monte Carlo treatment planning for photon and electron beams. *Radiat Phys Chem*. 2007;76(4):643-686.